Crystal Growth

Deutsche Ausgabe: DOI: 10.1002/ange.201604594
Internationale Ausgabe: DOI: 10.1002/anie.201604594

From Gold Nanoseeds to Nanorods: The Microscopic Origin of the Anisotropic Growth

*Santosh Kumar Meena and Marialore Sulpizi**

Abstract: *Directly manipulating and controlling the size and shape of metal nanoparticles is a key step for their tailored applications. In this work, molecular dynamics simulations were applied to understand the microscopic origin of the asymmetric growth mechanism in gold nanorods. Different factors influencing the growth were selectively included in the models to unravel the role of the surfactants and ions. In the early stage of the growth, when the seed is only a few nanometers large, a dramatic symmetry breaking occurs as the surfactant layer preferentially covers the (100) and (110) facets, leaving the (111) facets unprotected. This anisotropic surfactant layer in turn promotes anisotropic growth with the less protected tips growing faster. When silver salt is added to the growth solution, the asymmetry of the facets is preserved, but the Br^- concentration at the interface increases, resulting in increased surface passivation.*

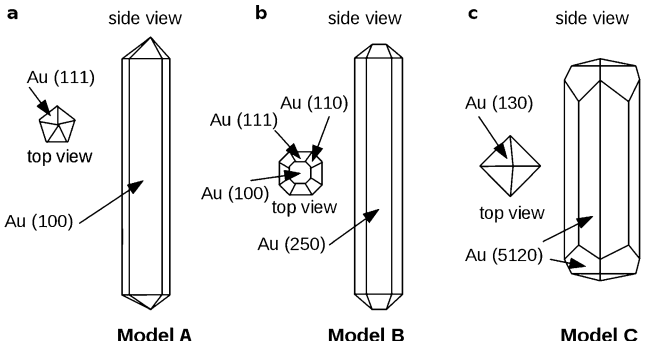

Figure 1. Schematic models for a) penta-twinned bipyramidal nanorods obtained in the absence of Ag^+, b) truncated hexagonal-bipyramidal nanorods obtained in the presence of Ag^+, and c) nanorods with eight Au(5120) lateral facets.[12]

Many applications of noble-metal nanoparticles in medical imaging, chemical sensing, and cancer treatment[1–5] require specific morphologies and dimensions. Plasmonic resonance responses and local field enhancements, for example, can be tuned through the particle size and shape. This has motivated intense research activities aiming to understand the growth mechanism of gold nanorods to control their morphology.

Gold nanorods are usually prepared according to a well established seed-mediated growth technique.[6–8] The final crystal morphology is the result of different factors, including the initial seed geometry, the interaction of ligands, and the presence of other additives that play a role in stabilizing certain crystallographic facets. Determining the crystal morphology of gold nanorods has been a major challenge owing to their small size. High-resolution transmission electron microscopy (HRTEM) studies have shown that nanorods prepared in the absence of Ag^+ have an idealized 3D prism morphology (penta-twinned decahedral) with five Au(111) facets at the two ends and five Au(100) side facets[9] (Figure 1 a).

Most gold nanorods are currently prepared with addition of silver nitrate to the growth solution as this can increase the yield of short gold nanorods (with an aspect ratio of ca. 6) to nearly 100 %.[7] The cross-section of the nanorods prepared by silver-assisted seeded growth can present more than one set of facet orientations depending on the growth parameters and can include low-index (100) and (110) planes[10] as well as high-index planes.[11,12] A nanorod geometry with eight identical high-index lateral Au(250) facets[11] is shown in Figure 1 b. A nanorod that consists of octagonal Au(5120) side facets, terminating in pyramids with Au(130) facets at the two ends that are connected to the sides by four small Au(5120) "bridging" facets,[12] is reported in Figure 1 c. Coexisting high- and low-index facets, namely an alternating sequence $(1+\sqrt{2},1,0)$, (110), $(1,1+\sqrt{2},0)$, (010), and so on, with comparable stability and dimensions have also been reported.[13]

These recent studies point to the fact that the interaction with surfactants and ions can lead to a reduction in the relative energy of a high-index facet. This suggests that growth can occurs on relatively open facets beyond the standard view that the most probable facets are also the most thermodynamically stable ones.

To understand the observed geometries, a key step is the microscopic analysis of the facet stabilization and the mechanism that induces the symmetry breaking from the initially isotropic seeds. Density functional theory (DFT) calculations have recently been used to show that surfactants, bromide, and silver preferentially adsorb on some facets of the seeds.[14] However, the cost of DFT calculations is still preventing the study of systems that include more than a few molecules. Force-field-based molecular dynamics (MD) simulations have proven to be effective for studying larger systems at the nanometer scale, including the electrolyte solution, and for accounting for the effect of temperature and dynamics on the nano- to microsecond timescale. In our recent work,[15,16] we have shown that the adsorption of surfactants on Au facets with different indices can lead to

[*] Dr. S. K. Meena, Prof. M. Sulpizi
Institute of Physics, Johannes Gutenberg University Mainz
Staudingerweg 7, 55099 Mainz (Germany)
E-mail: sulpizi@uni-mainz.de

Supporting information for this article can be found under: http://dx.doi.org/10.1002/anie.201604594.

different properties. Our atomistic simulations showed that on all surfaces, cetyltrimethylammonium bromide (CTAB) formed distorted cylindrical micelles spaced by water/ion channels, which can provide a path for the diffusion of the gold reactants towards the surface.[15] Moreover, CTAB formed a protective layer on Au(100) and Au(110) planes that is denser than that observed on the Au(111) surface, thus explaining why the Au(100) or Au(110) facets could grow more slowly, eventually resulting in anisotropic seed growth. Facet-specific coverage has also been observed for peptides on Pt nanoparticles.[17]

Describing nanoparticle facets as infinite planes is certainly appropriate when addressing a mature growth stage in which the nanorods have already reached a size larger than the micellar size, namely beyond 4–5 nm.[15,16] How would this picture change when considering smaller particles whose facets can be of the same size as the micelle, or even smaller? A detailed atomistic-scale investigation of the initial stages of gold nanorod growth has recently confirmed that the seed particles initially grow isotropically until a critical particle diameter of 4–6 nm is reached in the Ag^+ assisted growth solution.[18] This is exactly the size that we aim to investigate to understand the effect of the edges on the facet-dependent CTAB adsorption and to address the atomistic origin of the symmetry breaking.

The second key question is: How would CTAB adsorption change on the higher-index facets? In particular, how would the presence of higher-index facets challenge our explanation of the anisotropic growth based on the differences between (111) and (100) or (110) planes? To answer this question, we have investigated the adsorption of CTAB on Au(250), Au(130), and Au(5120) surfaces in the growth electrolyte solution.

Finally, the third objective of our work was to investigate the critical role played by the silver ions. To date, the exact role of silver in the anisotropic growth is still unclear. Part of the challenge stems from the difficulty to experimentally determine the silver oxidation state and the location of silver on the gold nanoparticles. We here aimed to investigate how silver addition modifies the structure of the protective layer on the gold surfaces.

We considered three models of gold nanoseeds: a cuboctahedron bound by (111) and (100) facets, which is the initial geometry of the seed before any truncation[18] (see the Supporting Information, Figure S1 a), a penta-twinned decahedron (Figure S1 b) with lateral (100) facets and tips formed by five twinned (111) facets, and a penta-twinned decahedral nanorod with an aspect ratio of 2:1 (Figure S1 c). Each of the nanoseeds was immersed in an orthorhombic box containing water, ions, and surfactants. As a starting point of all simulations, a uniform layer of CTAB, exceeding the critical micellar concentration, was built on all of the facets. The systems were equilibrated for a rather extended time on the order of a few microseconds. All MD simulations were performed with the GROMACS package (version 4.5.5),[19–22] using the CTAB force field from Ref. [23] and the Lennard–Jones parameters for gold from Heinz and co-workers[24] (for details of the simulations, see the Supporting Information). Snapshots of the three systems are shown in Figure 2 a–c, respectively.

In the case of the cuboctahedral seed, almost no micelle adsorption was observed on the Au(111) facets while micelle adsorption was observed on the Au(100) facets with a structure similar to that observed on the infinite planes. In Figure 2 d–f, the Br^- and CTA^+ surface densities on the different facets of the nanocrystals are reported as a function of the simulation time. The final surface densities of CTA^+ and Br^- are 1.49 and 1.53 ions nm^{-2} on the Au(100) facets, respectively (Table 1 and Figure 2 d). These values are very close to those determined for the infinite planes (Table 2) while the surface densities on Au(111) are negligible.

Table 1: Surface densities of CTA^+ and Br^- on the facets of the various nanostructures. The maximum standard error is 0.05 ions nm^{-2}.

Structure	CTA^+ [ions nm^{-2}]	Br^- [ions nm^{-2}]
cuboctahedral nanoseed, Au(100)	1.49	1.53
cuboctahedral nanoseed, Au(111)	0.18	0.19
penta-twinned nanoseed, Au(100)	1.62	1.62
penta-twinned nanoseed, Au(111)	0.19	0.30
penta-twinned nanorod, Au(100)	1.53	1.48
penta-twinned nanorod, Au(111)	0.30	0.16

Table 2: Surface densities of CTA^+ and Br^- and widths of the water ion channels on different gold surfaces.[a]

Surface	Au(111)	Au(110)	Au(100)	Au(250)	Au(130)	Au(5120)
CTA^+ [ions nm^{-2}]	1.31	1.49	1.49	1.38	1.50	1.62
Br^- [ions nm^{-2}]	1.09	1.41	1.40	1.53	1.46	1.55
channel width [nm]	0.94	0.71	0.73	0.56	0.65	0.60

[a] The data for Au(111), Au(110), and Au(100) were taken from Ref. [15].

For the penta-twinned seeds, similar results were obtained. On the lateral Au(100) facets, micelles clearly adsorb with a structure similar to that observed on the infinite planes while the situation is dramatically different on the tips. Indeed, no clear micellar adsorption was observed on the inter-twinned Au(111) surfaces. The surface densities of CTA^+ are 1.62 and 1.53 ions nm^{-2} on the Au(100) facets of the nanoseed and nanorod, respectively (Table 1). These values are very close to those on the infinite planes (Table 2).

Our simulations suggest that at an early stage, when the seed dimensions are comparable to those of the micelles, a strong anisotropy is built up between the facets, which in turn results in unprotected Au(111) facets, where faster growth should be possible. In the case of the penta-twinned seeds, this anisotropy would then favor the growth of elongated rods (such an argument would not hold for the

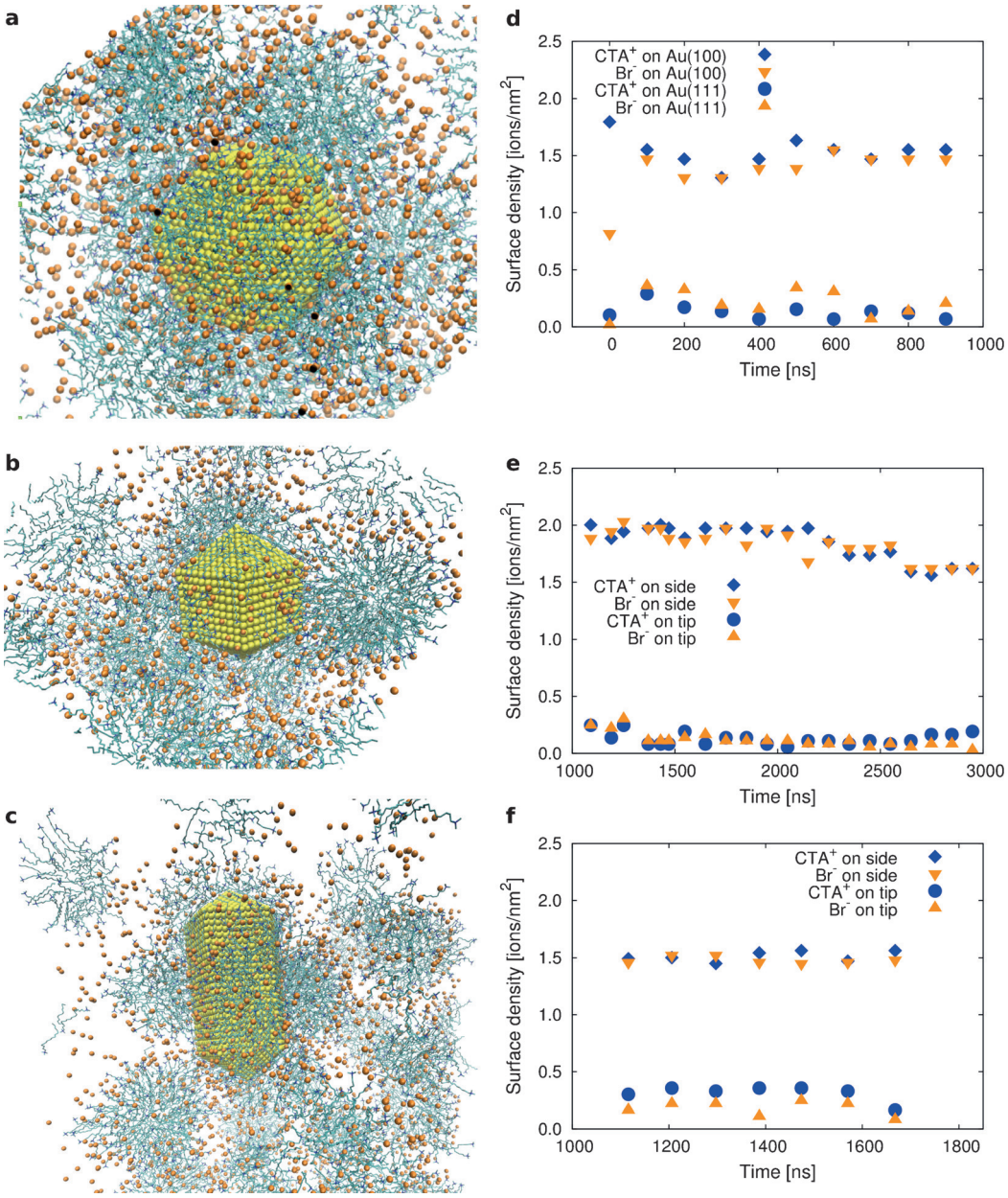

Figure 2. Snapshots of a) the cuboctahedral nanoseed (after 900 ns), b) the penta-twinned nanoseed (after 2950 ns), and c) the nanorod (after 1668 ns) in CTAB solution (water molecules omitted for clarity). Surface densities on the lateral sides and tips of d) the cuboctahedral nanoseeds, e) the penta-twinned nanoseeds, and f) the nanorods as a function of time.

cuboctahedral seed where growth of the (111) facets would result in a cube).

As already described in the introduction, rods can exhibit higher-index facets. In Figure 3, the CTAB layers adsorbed on different facets are compared. We generally found that on the higher-index facets, the adsorbed micelles have a structure rather similar to that on the lower-index facets although the overall surfactant layer appears to be flatter and more compact. Looking at the Br^- density (solid orange line in Figure 3 f–h), we found that Br^- ions can adsorb in the gaps available on the more open surfaces, resulting in a broader peak that is closer to the higher-index facets than to Au(111). The CTA^+ density (solid blue line) follows the Br^- density profile, also resulting in broader peaks for the higher-index facets. On Au(110), Au(100), Au(250), Au(130), and Au(5120), the Br^- density is approximately 1.4–1.5 ions nm^{-2}, which is higher than the value of 1.1 ions nm^{-2} obtained for Au(111) (Table 2). The surface density of CTA^+ is also higher on the higher-index facets except for Au(250) (in the range of 1.4–1.6 ions nm^{-2} for Au(110), Au(100), Au(250), Au(130), and Au(5120)) and higher than the value of 1.3 ions nm^{-2} measured for Au(111). The denser ion coverage on the higher-index surfaces could, in turn, be responsible for a lower ion diffusion flux towards such surfaces. This would suggest that in all of the considered rod models (a–c) in Figure 1, the lateral facets would be more protected by the surfactants than the tips, allowing for the anisotropic growth. Finally, the water/ion channels between the micelles are narrower on the

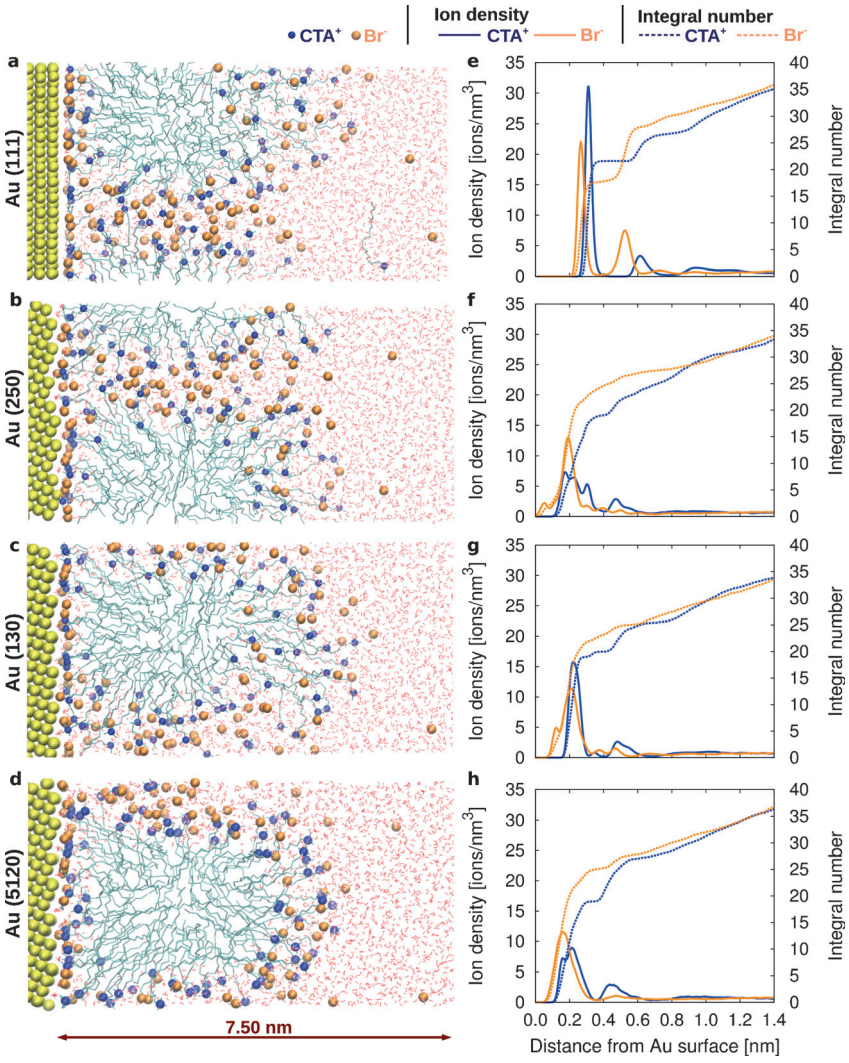

Figure 3. Snapshots from the simulations for a) Au(111), b) Au(250), c) Au(130), and d) Au(5120). Ion densities and integral numbers as a function of the distance from the surface for e) Au(111), f) Au(250), g) Au(130), and h) Au(5120).

higher-index facets than on the lower-index facets (Figure S4 and Table 2). This would eventually lead to faster diffusion of the gold reactants towards the Au(111) surface than towards the higher-index facets.

How is the depicted scenario modified upon addition of silver salt? In silver-assisted seed-mediated growth, the presence of 5% Ag^+ already increases the yield of the gold nanorods to nearly 100% although higher concentrations (comparable to the CTAB concentration, 0.1M) of Ag^+ have also been used.[7] However, the actual concentration at the interface, namely the Ag^+ surface density, has not been determined experimentally. Given the high propensity of Ag^+ to adsorb on gold surfaces, it is expected that even in the presence of a relatively low concentration of $AgNO_3$ in the electrolyte solution, the surface concentration of Ag^+ may be quite high. In our simulations, we considered an electrolyte solution containing a AgBr amount that corresponds to 20% of the CTAB amount. In our model, Ag^+ and Br^- are adsorbed on the surface in ionic form, and silver reduction was not considered.

Ag^+ is directly adsorbed on the gold surfaces and forms, together with Br^-, the first adsorbed layer (gray line, Figure S5 f–h). The Ag^+ adsorption leads to a higher concentration of Br^- on the surface than in the absence of Ag^+. In fact, on Au(111), the Br^- surface density is increased from 1.09 ions nm^{-2} in the absence of silver to 2.14 ions nm^{-2} in the presence of silver. Overall, on all three planes, passivation by the Br^- ions is increased. Whereas the CTA^+ surface densities are similar on Au(111), Au(110), and Au(100), the Br^- surface density is higher on Au(110) than on Au(111). Aside from the increased surface passivation, the preferential silver adsorption (in the order (110) > (100) > (111)) will slow down further gold deposition, as the surface energy of silver is 15% lower than that of gold. Such an argument was also used in Ref. [25] to explain the anisotropic growth of metal particles in ionic liquids.

The results from the simulations suggest that in the early stage of the growth, when the seed is only a few nanometers large, a dramatic symmetry breaking can occur. The surfactant layer preferentially covers the (100) and (110) facets, leaving the (111) facets unprotected. In the case of penta-twinned nanocrystals, for example, CTAB micelles adsorb on the lateral Au(100) facets with a structure similar to that observed on the infinite plane while no micellar adsorption is observed on the tips. The anisotropic surfactant distribution in turn promotes anisotropic growth, with the less protected tips growing faster. Some higher-index facets that have also been experimentally observed in the mature nanorods behave similar to the low-index (100) and (110) facets, but are at odds with respect to Au(111).

Finally, we investigated how the picture described thus far changes upon addition of a silver salt to the solution. Silver ions have a strong propensity for the gold surface where they can form AgBr islands with different specific geometries depending on the surface plane. Although the structure of the surfactant layer is similar to that in the absence of silver, silver substantially increases the Br^- concentration at the interface, resulting in increased surface passivation.

In conclusion, our work has shed new light on the microscopic structure of the nanorods and electrolyte solution, dissecting the roles of the different components, including the shapes of the nanoparticles at an early growth stage, the higher-index facets, and the silver ions, in the anisotropic growth process. Our work paves the way for further simulations in this area, which will include gold reduction at the interface.

Acknowledgements

We thank C. Sönnichsen, U. Kolb, and S. Link for useful discussions and the Deutsche Forschungsgemeinschaft for financial support (SU 752/1). The simulations were performed on the ZDV Mogon cluster.

Keywords: adsorption · crystal growth · interfaces · molecular dynamics · nanoparticles

How to cite: *Angew. Chem. Int. Ed.* **2016**, *55*, 11960–11964
Angew. Chem. **2016**, *128*, 12139–12143

[1] Y. Xia, Y. Xiong, B. Lim, S. Skrabalak, *Angew. Chem. Int. Ed.* **2009**, *48*, 60–103; *Angew. Chem.* **2009**, *121*, 62–108.
[2] D. A. Giljohann, D. S. Seferos, W. L. Daniel, M. D. Massich, P. C. Patel, C. A. Mirkin, *Angew. Chem. Int. Ed.* **2010**, *49*, 3280–3294; *Angew. Chem.* **2010**, *122*, 3352–3366.
[3] X. Huang, I. H. El-Sayed, M. A. El-Sayed, *Methods Mol. Biol.* **2010**, *624*, 343–357.
[4] A. M. Alkilany, L. B. Thompson, S. P. Boulos, P. N. Sisco, C. J. Murphy, *Adv. Drug Delivery Rev.* **2012**, *64*, 190–199.
[5] P. D. Howes, R. Chandrawati, M. M. Stevens, *Science* **2014**, *346*, 53–63.
[6] N. R. Jana, L. Gearheart, C. J. Murphy, *J. Phys. Chem. B* **2001**, *105*, 4065–4067.
[7] C. J. Murphy, T. K. Sau, A. M. Gole, C. J. Orendorff, J. Gao, L. Gou, S. E. Hunyadi, T. Li, *J. Phys. Chem. B* **2005**, *109*, 13857–13870.
[8] B. Nikoobakht, M. A. El-Sayed, *Chem. Mater.* **2003**, *15*, 1957–1962.
[9] C. J. Johnson, E. Dujardin, S. A. Davis, C. J. Murphy, S. Mann, *J. Mater. Chem.* **2002**, *12*, 1765–1770.
[10] B. Goris, S. Bals, W. V. den Broek, E. Carbo-Argibay, S. Gomez-Grana, L. M. Liz-Marzan, G. V. Tendeloo, *Nat. Mater.* **2012**, *11*, 930–935.
[11] E. Carbó-Argibay, B. Rodríguez-González, S. Gómez-Graña, A. Guerrero-Martínez, I. Pastoriza-Santos, J. Pérez-Juste, L. M. Liz-Marzán, *Angew. Chem. Int. Ed.* **2010**, *49*, 9397–9400; *Angew. Chem.* **2010**, *122*, 9587–9590.
[12] H. Katz-Boon, C. J. Rossouw, M. Weyland, A. M. Funston, P. Mulvaney, J. Etheridge, *Nano Lett.* **2011**, *11*, 273–278.
[13] H. Katz-Boon, M. Walsh, C. Dwyer, P. Mulvaney, A. M. Funston, J. Etheridge, *Nano Lett.* **2015**, *15*, 1635–1641.
[14] N. Almora-Barrios, G. Novell-Leruth, P. Whiting, L. M. Liz-Marzán, N. López, *Nano Lett.* **2014**, *14*, 871–875.
[15] S. K. Meena, M. Sulpizi, *Langmuir* **2013**, *29*, 14954–14961.
[16] S. K. Meena, S. Celiksoy, P. Schaefer, A. Henkel, C. Sönnichsen, M. Sulpizi, *Phys. Chem. Chem. Phys.* **2016**, *18*, 13246–13254.
[17] H. Ramezani-Dakhel, L. Ruan, Y. Huang, H. Heinz, *Adv. Funct. Mater.* **2015**, *25*, 1374–1384.
[18] M. J. Walsh, S. J. Barrow, W. Tong, A. M. Funston, J. Etheridge, *ACS Nano* **2015**, *9*, 715–724.
[19] H. Berendsen, D. van der Spoel, R. van Drunen, *Comput. Phys. Commun.* **1995**, *91*, 43–56.
[20] D. Van Der Spoel, E. Lindahl, B. Hess, G. Groenhof, A. E. Mark, H. J. C. Berendsen, *J. Comput. Chem.* **2005**, *26*, 1701–1718.
[21] B. Hess, C. Kutzner, D. V. D. Spoel, E. Lindahl, *J. Chem. Theory Comput.* **2008**, *4*, 435–447.
[22] S. Pronk, S. Pall, R. Schulz, P. Larsson, P. Bjelkmar, R. Apostolov, M. R. Shirts, J. C. Smith, P. M. Kasson, D. van der Spoel, B. Hess, E. Lindahl, *Bioinformatics* **2013**, *29*, 845–854.
[23] Z. Wang, R. G. Larson, *J. Phys. Chem. B* **2009**, *113*, 13697–13710.
[24] H. Heinz, R. A. Farmer, R. R. Naik, *J. Phys. Chem. B* **2008**, *112*, 17281–17290.
[25] K. Jha, H. Liu, M. Bockstaller, H. Heinz, *J. Phys. Chem. C* **2013**, *117*, 25969–25981.

Received: May 11, 2016
Revised: July 21, 2016
Published online: August 25, 2016

